Available online at www.sciencedirect.com

ScienceDirect

Energy Procedia 77 (2015) 129 – 138

Energy Procedia

5th International Conference on Silicon Photovoltaics, SiliconPV 2015

Simulation study of multi-wire front contact grids for silicon solar cells

Massimo Nicolai[a], Mauro Zanuccoli[a], Paolo Magnone[b], Marco Galiazzo[c], Diego Tonini[c], Matteo Bertazzo[c], Enrico Sangiorgi[a], Claudio Fiegna[a]

[a]*Advanced Research Center on Electronic-System (ARCES), and Department of Electrical, Electronic, and Information Engineering "Guglielmo Marconi" (DEI) University of Bologna, Via Venezia 52, Cesena (FC) 47521, Italy*
[b]*DTG, University of Padova, Stradella S. Nicola, 3 I-36100 Vicenza, Italy*
[c]*APPLIED MATERIALS ITALIA s.r.l., Olmi di S. Biagio di Callalta (TV) 31408, Italy*

Abstract

Multi-wire (MW) front-contact schemes represent a promising alternative to standard H-pattern structure with ribbon busbar (BB) in silicon solar cells. In the case of MW schemes, busbar are replaced by copper wires. MW have been demonstrated to enhance the photo-generation with respect to a standard H-pattern structure with ribbon busbar when solar cells are encapsulated and assembled in modules. However, the influence of the geometrical and optical properties of the encapsulation layers as well as of wires on the optical effective shading is not exhaustively treated by the literature. In this work, we have performed electro-optical simulations of MW and BB based solar cells in order to calculate the effective optical shading factor, the enhancement of conversion efficiency and the saving of contact-paste, with respect to the BB design. Specifically, we have studied by means of a ray-tracing simulation tool the significant impact of the front contact grid geometry, of the encapsulation layer thickness and of the optical properties of the cell front interface on the effective optical shading. The calculated values of effective optical shading are used to determine the enhancement of the figures of merit and the paste saving with respect to the reference silver BB scheme. On the basis of our calculations the adoption of optimized MW designs may enhance the conversion efficiency up to 0.5 $\%_{abs}$, allowing paste saving up to 50 mg per cell.

Peer review by the scientific conference committee of SiliconPV 2015 under responsibility of PSE AG

Keywords: Multi-Wire MW Scheme, Electro-Optical Simulation, Effective optical shading

Peer review by the scientific conference committee of SiliconPV 2015 under responsibility of PSE AG
doi:10.1016/j.egypro.2015.07.020

1. Introduction

Conventional industrial H-pattern silicon solar cells adopt a grid of screen printed busbar and fingers fabricated starting from silver pastes. Inside PV modules, solar cells are encapsulated by a layer stack of glass and a polymeric material.

The total fabrication cost of the module is markedly sensitive to the amount of silver-based paste used for the front-contact grid. With this regard, the silver (Ag) paste consumption of industrial screen-printed crystalline silicon solar cells is within the range 120 mg - 200 mg per wafer [1]. In the recent years, one challenging task for photovoltaic industry is to reduce the consumption of Ag paste. However, paste saving techniques are often associated to an increase of total series resistance leading to Fill-Factor (FF) degradation and significant power loss. Moreover, the front-grid design has a marked impact in terms of light shading losses [2].

Multi-wire (MW) schemes [3,4] represent an alternative option to BB aimed at reducing the silver paste consumption in silicon solar cells. In the case of MW schemes, busbar are replaced by copper wires resulting in paste saving. MW are promising for the silicon solar cell industry. In fact, due to their geometry, MW lead to photo-generation enhancement with respect to standard ribbon busbar [5] thanks to a better light-trapping within the cell layer stack consisting of glass, encapsulant and silicon. Moreover, MW are straightforwardly implementable on existing cells offering a full compatibility with different device architectures. In particular, only a few technical details of the process have to be modified, by using a different kind of cell stringer [3].

Optical simulations of MW can be helpful in order to study the light trapping properties of the MW scheme. Several authors have theoretically and experimentally studied the effective optical shading of encapsulated solar cells featuring aerosol-printed and plated fingers presenting a circular cross-section similar to that of copper wires [6]. They reported that the effective optical shading ranges between one third to half of the wire diameter. Blakers [6] has calculated the effective shading of a rough half-circular encapsulated finger and, by a comparison to reflection measurements, he presented experimental data to support calculations of the effective optical shading. In [5], the effective reflection on different types of metal fingers has been analysed by theory and experiments. However, to our knowledge, one issue that has not been addressed to date is that of the sensitivity of the effective optical shading of wires to their geometry and density, to the thickness of the encapsulant layer as well as to the optical reflectance of the cell front interface. The influence of these parameters on the light trapping enhancement due to MW may have a relevant impact on the cell design.

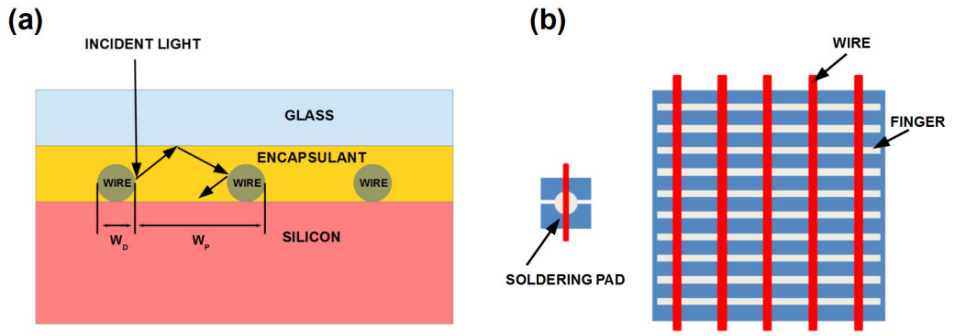

Fig. 1. (a) Sketch of the encapsulated multi-wire solar cell (cross-section, not to scale) and (b) top view schematic of the contacting grid with the detail of a soldering pad.

In this work, we have performed electro-optical simulations of MW and BB based solar cells in order to calculate the effective shading factor, the enhancement of conversion efficiency and the paste saving of the MW scheme with respect to the BB design. In particular, by means of optical simulations, we have analyzed the impact of the geometries of the stack layer, of the wire coverage fraction and diameter, and of cell front reflectivity on the wire

effective optical shading. An extensive analysis of different wire diameters has been carried out investigating coverage fraction values up to 20 %.

The remainder of the paper is organized as follows. In section 2, we describe the simulation methodology. In section 3.1, we discuss the results of the effective shading of copper wires in the case of encapsulated industrial crystalline silicon solar cells calculated by means of a ray-tracing simulation tool. In section 3.2, we have used the calculated values of optical effective shading to determine the conversion efficiency enhancement with respect to the reference silver BB scheme, and to calculate the paste saving achievable by the adoption of the MW schemes. Finally, in section 4, the main conclusions of the paper are reported.

2. Simulation methodology and studied solar cells

In this study, we consider a stack of a 3.2 mm-thick glass layer and 450 μm-thick encapsulant (Fig. 1a), representing typical values adopted in commercial modules [7]. Figure 1b shows a schematic top view of the cell where standard silver busbar are replaced by copper wires. The two-dimensional simulation domain is the half of the wire pitch W_P. Mirror and absorbing boundary conditions have been assumed at sides and at bottom of the domain, respectively. The considered c-Si solar cell features a p-type 180 μm-thick substrate with 1.5 Ωcm resistivity. A 75 Ω/sq phosphorous doped homogeneous emitter and an aluminium back surface field (Al-BSF) have been assumed [8]. The size of the cell is 15.6 cm x 15.16 cm.

Optical simulations have been performed by using a standard raytracer [9] and by considering either a textured front interface with regular upright pyramids or a simpler planar surface. In both cases, the cell is coated by a 75 nm-thick silicon nitride layer. We impose at the silicon/encapsulant interface the wavelength-dependent reflectivity calculated separately. The assumed wavelength span for the simulation is 30 nm, which has been previously validated as a good trade-off between computational effort and accuracy. The rays distribution is non-uniform to save memory and to reduce the computation time. In particular, the spatial ray density is higher in regions close to the wires (minimum spacing 0.1 μm) while in the mid region between wires the maximum ray spacing is 1 μm. We assume that the reflectivity of the encapsulant-wire interface is equal to 1. This assumption has been done in order to study the impact of the circled shape respect to the standard geometry and to compare the values obtained from the simulations with those reported in the literature. Therefore, the wavelength dependence of the Copper/Encapsulant interface has not been considered and this leads to an overestimation of the calculated optical parameters. In particular, we observe an increase of 0.7 $\%_{rel}$ for the optical shading factor values with respect to the wavelength dependent cases. The optical properties of glass and encapsulant are modelled according to [10] and [11], respectively. The wire effective optical shading factor $K_{shading}$ is defined as:

$$K_{shading} = \frac{W'}{W_D} \tag{1}$$

where W_D is the wire diameter and W' is the width of the ideal planar finger providing the same photo-generated current density (J_{PH}) obtained by the wire scheme. The relative enhancement of photo-generated current ($J_{PH,Enh}$) due to the MW scheme is:

$$J_{PH,\,Enh} = \frac{J_{PH} - J_{PH,\,ideal}}{J_{PH,ideal}} \tag{2}$$

where J_{PH} and $J_{PH,ideal}$ are the photo-generated current densities in the case of wires and in the case of ribbon busbar with ideal optical shading $K_{shading} = 1$, respectively.

In order to calculate the photo-generated current density we consider the standard reference spectrum ASTM AM1.5G [12] and 1000W/m^2 irradiance, with light normally incident on the device plane. Electrical simulations have been performed with the calculated effective shading of copper wires $K_{shading}$ in order to determine the conversion efficiency enhancement for the MW cases with respect to the reference silver BB scheme (3, 4 and 5 BB). In the MW cases, the optimum number of wires (N_W) is evaluated as the one providing the maximum conversion efficiency. We explore a reasonable range of N_W (from 3 to 50) (subsection. 3.2) and we observe that it is strongly dependent on the number of busbar and on the wire diameter. For ribbon busbar and wires soldering pads (size set to 1.5 times the wire diameter) we assume ideal shading and for silver fingers an effective shading factor equal to 0.42 [5]. This assumption is realistic by considering the aspect ratio and the geometry of fingers and pads. The current-voltage characteristics under illumination accounting for optical shading and contact by fingers as well as for emitter resistance have been performed by using a drift diffusion simulator as described in [13-17] and accounting for physical models as described in [18]. The contribution of the contact grid resistance to the total series resistance as well as the optical shading due to busbar for the reference design or due to wires in the case of MW are accounted for in post-processing by properly correcting the I-V characteristic. In this study, we assume a fixed total coverage fraction of the silver busbar for the reference design (2.88 %). We set the finger height to 13 µm in the case of BB scheme. According to the number of BB and to the finger width (in this paper we consider the following finger widths: 25 µm, 45 µm, 65 µm, 85 µm), the number of fingers has been optimized allowing a fair comparison between different grid configurations. The optimum number of fingers varies within the range 74 - 150. In the calculation of the total series resistance, we include the emitter and the contact resistance, the grid contribution and the resistance due to cell interconnect wires [19]. Such interconnect wire is assumed to be 1 cm-long and 200 µm-thick.

In order to calculate the silver paste savings due to the MW schemes, the fingers past consumption has been determined by assuming a 7 mg/mm^3 silver paste [20]. This results in a total paste weight of 167 mg for a wafer featuring W_F = 25 µm and 3 BB, comparable to values reported in [1,3-4].

3. Results and discussion

3.1 Optical simulation: effective optical shading for wires

3.1.1 Spectral dependence of the photo-current density enhancement

Fig. 2 shows the radiation wavelength (λ) dependence of the photogenerated current density enhancement $J_{PH,Enh}$ with respect to the reference silver-BB case.

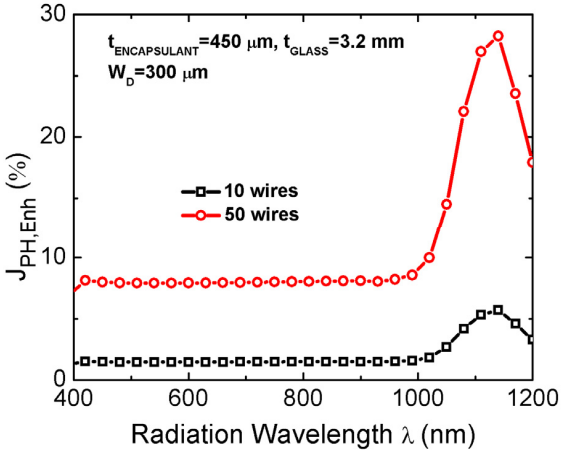

Fig. 2. Wires-related photo-generated current enhancement ($J_{PH,Enh}$) versus the radiation wavelength (λ) for two different number of wires: 10 and 50. $t_{ENCAPSULANT}$, t_{GLASS} and W_D are the encapsulant thickness, the glass thickness and the wire diameter, respectively.

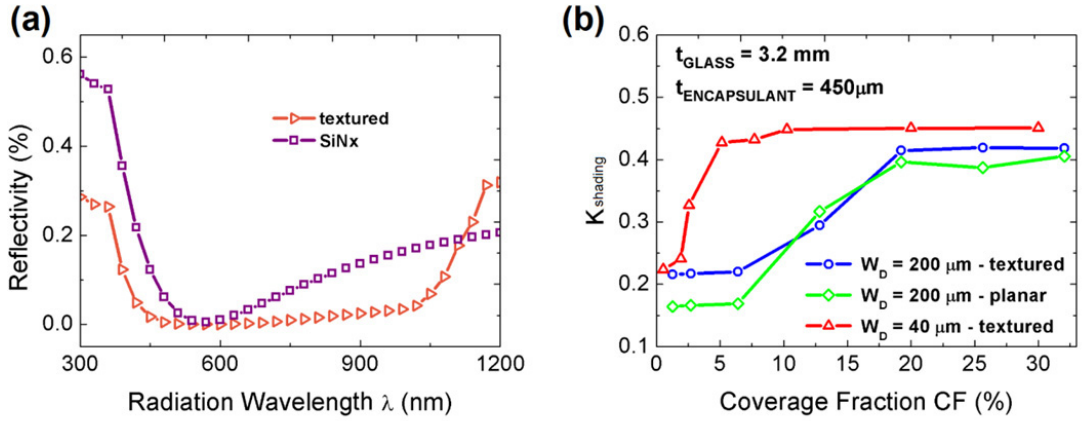

Fig. 3. (a) Reflectivity (measured) versus radiation wavelength (λ) in the case of textured and planar front interface, both coated by 75 nm-thick silicon nitride (SiNx) and (b) effective optical shading factor $K_{shading}$ for wire diameter W_D = 200 μm (textured and planar front interface) and W_D = 40 μm (textured front interface). Calculations have been carried out assuming glass thickness t_{GLASS} = 3.2 mm and encapsulant thickness $t_{ENCAPSULANT}$ = 450 μm.

We observe that $J_{PH,Enh}$ is approximately constant for λ below 1000 nm due to the weak dependence on photon energy of the optical properties of materials and surface reflectivity. For λ > 1000 nm, the effectiveness of the light scattering is more pronounced and is affected by a significant dependence of front reflectivity on wavelength.

By increasing the number of wires from 10 to 50, $J_{PH,Enh}$ increases due to the stronger mutual influence among wires. Indeed, simulations show that a higher number of wires leads to increased optical absorbance in silicon combined with lower parasitic absorption in the encapsulant layer. Overall, this results in a lower external reflectance.

It is worth noting that, despite $J_{PH,Enh}$ is higher in the case of denser wire grid (50 wires), the influence on J_{PH} is compensated by a higher coverage fraction (CF) which leads to more optical shading. For instance, with W_D = 300 μm, J_{PH} decreases from 37.56 mA/cm^2 to 36.97 mA/cm^2 (-1.5 $\%_{rel}$) when N_W increases from 10 to 50. Despite this, from Fig. 2, the expected relative increase in J_{PH} is approximately 7 % for higher N_W. However, higher N_W results in lower total series resistance, as discussed in subsection 3.2.

3.1.2 Influence of front reflectivity, wire diameter and wire coverage fraction on the effective optical shading

Two markedly different reflectivity characteristics at the front interface have been analyzed, one for textured interface and the second for planar interface, both coated by 75 nm-thick silicon nitride (called SiN_x) (Fig. 3a). As expected, the textured cell exhibits a significantly lower reflectance. Fig. 3b shows the optical shading versus the wire CF. We observe that for a given wire diameter (W_D = 200 μm) at relatively lower CF (corresponding to a number of wires N_W up to 50) the light trapping due to encapsulated MW is more effective in the case of planar front interface ($K_{shading}$ = 0.16) as compared to the textured case ($K_{shading}$ = 0.22). Indeed, higher incident power is reflected by the planar front interface resulting in an enhanced scattering from the encapsulant/wire interface although, due to the strong difference in average reflectivity, the textured morphology results in higher J_{PH} (+5.2 $\%_{rel}$). For CF-values above 7 % the influence of the front interface reflectivity is less relevant probably due to the reduced wire spacing. In addition, we observe that, at fixed CF, $K_{shading}$ is strongly dependent on wire diameter. As it can be observed in Fig. 3b, from the optical point of view, MW schemes take advantage from higher diameters, especially when CF is lower than 20 %. Probably this is due to the larger rounded cross section surface area of the wire, which plays a role in lowering $K_{shading}$.

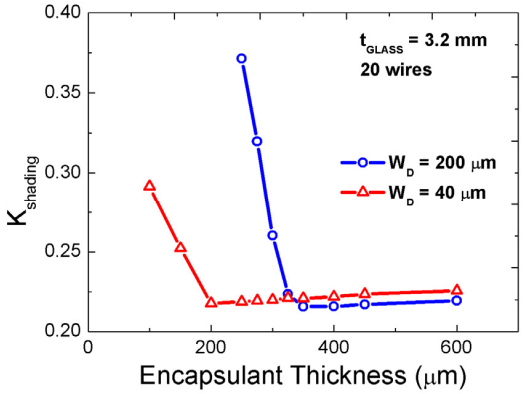

Fig. 4. Effective optical shading factor $K_{shading}$ versus encapsulant thickness $t_{ENCAPSULANT}$ for wire diameter W_D = 200 μm and W_D = 40 μm with glass thickness t_{GLASS} = 3.2 mm and for 20 wires.

Table 1. Materials parameters used in the calculations.

Parameter	Value
Silver resistivity (Ω·cm)	$2.7 \cdot 10^{-6}$
Copper resistivity (Ω·cm)	$1.69 \cdot 10^{-6}$
Specific front contact resistivity (Ω·cm^2)	$1 \cdot 10^{-3}$
Emitter sheet resistance (Ω/sq)	75

The calculated values of effective optical shading factor $K_{shading}$ = 0.22 (CF up to 3 %), and $K_{shading}$ = 0.46 (W_D = 40 μm, CF = 10 %) are comparable to those discussed in [21]. In addition, on the basis of our simulations, for CF lower than 3 %, $K_{shading}$ is not markedly affected by the wire diameter. This is relevant for the front grid design since, as it will be shown in subsection 3.2, the optimum CF corresponding to the peak conversion efficiency is relatively low.

3.1.3 Influence of encapsulation stack geometry

Simulations show that $K_{shading}$ is dependent on the geometry of the material stack, in particular on the encapsulant thickness $t_{ENCAPSULANT}$. Fig. 4 shows that for a number of wires comparable to the optimum one (about 20 wires, Subsection 3.2) and glass thickness equal to 3.2 mm (W_D = 200 μm and W_D = 40 μm), $K_{shading}$ is markedly dependent on the encapsulant thickness, when its value is comparable with W_D. However, when $t_{ENCAPSULANT}$ is several times W_D, the influence of the encaplsulant layer thickness is not appreciable. Therefore, in order to reduce the material cost, for W_D within the range 100 μm – 300 μm an encapsulant layer thickness of 400 μm is enough to ensure a low $K_{shading}$.

3.2 Electrical simulation: calculation of the solar cell main figures of merit under illumination

We have calculated the optimum number of wires for different diameters and compared the main figures of merit of the solar cell with those of the reference grid design. For the reference scheme we assume 3, 4, and 5 silver BB. Calculations have been performed for finger width W_F from 25 μm to 85 μm and for wire diameter W_D from 100 μm to 400 μm. The materials parameters used in the calculations are summarized in Table 1.
Fig. 5 illustrates the contributions to the series resistance due to fingers, wires, busbar and the cell interconnect wires. We observe that the most relevant contribution is that of wires in the case of MW, while the finger resistance has a minor impact.

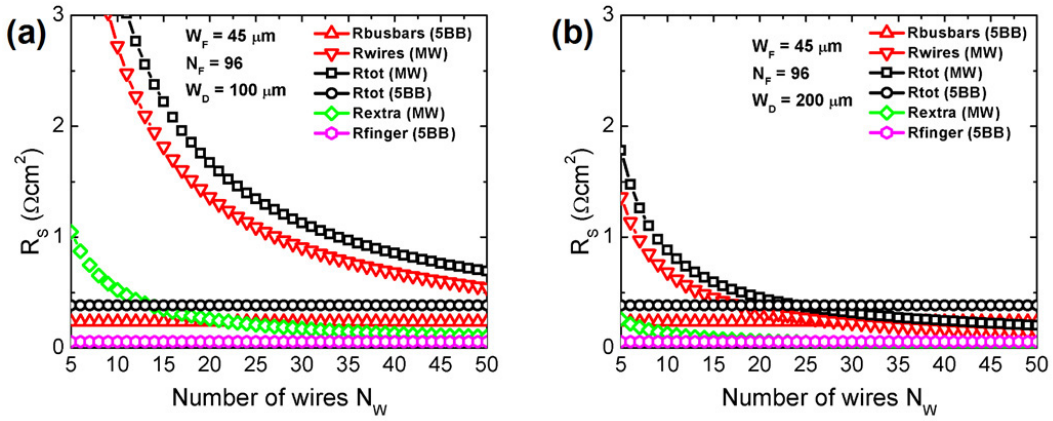

Fig. 5. Significant calculated contributions to the total parasitic resistance per unit area in the case of multi-wire and busbar grids. Two wire diameters W_D are illustrated: (a) 100 μm and (b) 200 μm. R_{extra} denotes the cell interconnect wires contribution to the total resistance. The contribution of the metal-semiconductor contact resistance [19] is negligible and other types of contact have not been considered.

For this reason, in order to save paste, we have decreased the finger thickness to 6.75 μm in the case of MW respect to the thickness of 13 μm in the case of silver BB.

In our simulations, in terms of loss parameters, we consider an infinite shunt resistance and the same saturation current density for each configuration of number of finger (N_F) and respective width (W_F).

The performance of the cell are valued considering the Fill Factor (FF) and the conversion efficiency.The FF is a parameter which, in conjunction with the short-circuit current (J_{SC}) and the open circuit voltage (V_{OC}), determines the maximum power from a solar cell. The FF is calculated starting from the simulated I-V characteristic which allows to obtain the maximum power point (P_{mpp}). The P_{mpp} is degraded by parasitic resistive losses (Fig. 5) and when the value of the parasitic resistance (strongly influenced by the wire contribution while other components such as the resistance of the finger and the cell interconnect wires contribution R_{extra} have a minor impact) is considerable a FF degradation might be observed (Fig. 6 and 7). More in detail, in the case of wire diameter W_D = 100 μm, a relatively relevant wire contribution to the total parasitic resistance (Fig. 5a) due to the low value of the diameter, leads to strong FF degradation (Fig. 6a and 7a) which does not allow an efficiency enhancement with respect to the BB design (Fig. 6b and 7b). This does not occur for larger W_D (Fig. 5b).

Moreover, even the conversion efficiency is limited due to the resistive losses and a trade-off between light shading and resistance of the front contact might be considered to obtain the maximum efficiency. In fact, if the wire diameter W_D increases, a lower number of wires N_W is requested to obtain the maximum efficiency (Fig. 6 and 7).

It is worth noting that the efficiency enhancement of the MW cell with respect to the BB option depends on wire diameter, fingers width and number of BB of the baseline (Fig. 6 and 7). Indeed, the higher is the number of BB, the lower is the resistance of fingers, leading to higher efficiency of the baseline (BB-cell).

The efficiency increases up to 0.37 $\%_{abs}$ with respect to the 5 BB design (W_D = 300 μm, W_F = 45 μm) and up to 0.5 $\%_{abs}$ compared to 3 BB reference. In the last case, the silver paste consumption decreases from 123 mg to 30 mg per wafer assuming a paste density of 7 mg/mm^3 (for standard single-print screen printed cells is between 120 mg and 200 mg [1]).

A further interesting aspect is the analysis of the impact of the encapsulant stack. In Fig. 8 the calculated short-circuit current density J_{SC} versus the number of wires for encapsulated MW cells is compared to that without encapsulant and glass for wire diameter W_D = 300 μm and finger width W_F = 45 um.

In addition, the comparison with a three busbar (3 BB) solar cell is illustrated. We observe that at the optimum number of wires in terms of efficiency (N_W = 19 for encapsulated cell and N_W = 8 non-encapsulated cell), J_{SC} is higher in the case of MW thanks to optical effects resulting from the adoption of a circular shape (wire). Moreover, the gain in terms of J_{SC} is higher in the case of encapsulated cell thanks to the advantages provided by this stack [11].

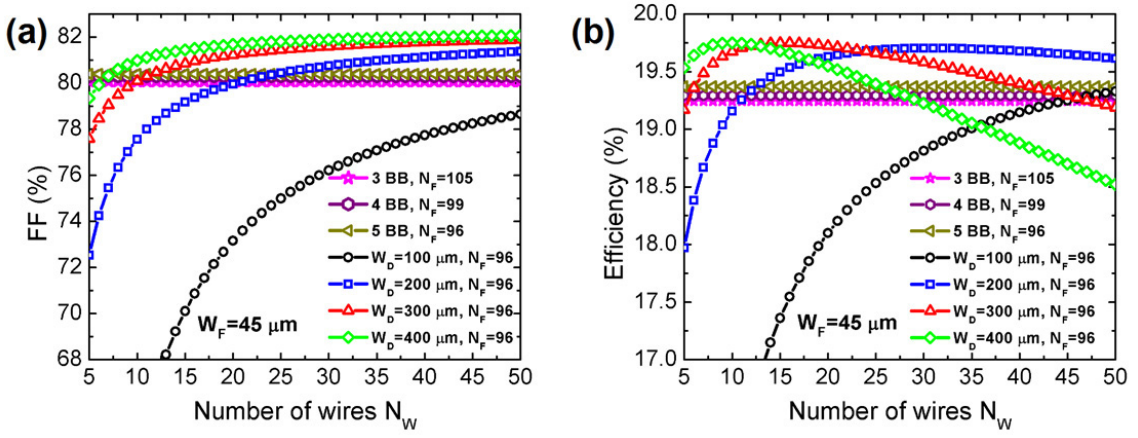

Fig. 6. Calculated Fill Factor (a) and efficiency (b) in the case of multi-wire and busbar (3, 4, 5 BB) schemes for finger width W_F = 45 μm. Multi-wire have been simulated assuming 96 fingers, while BB solar cells with an optimized number of fingers N_F.

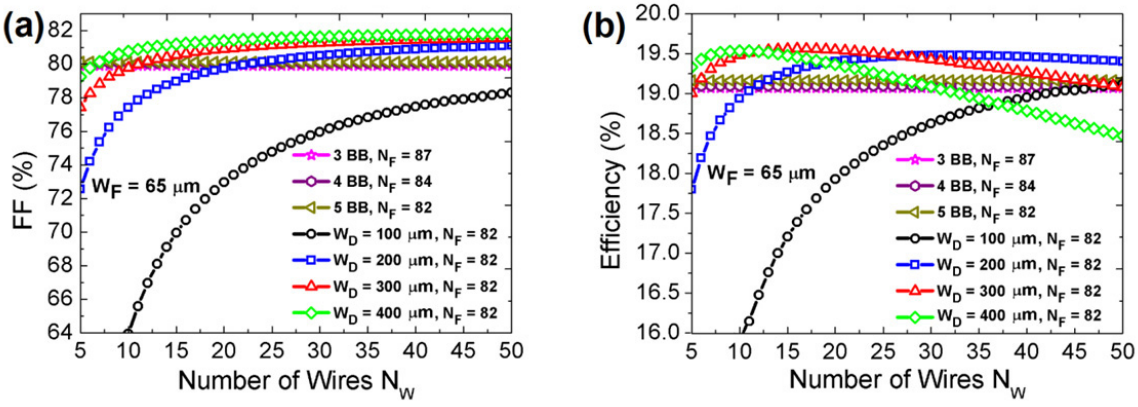

Fig. 7. Calculated Fill Factor (a) and efficiency (b) in the case of multi-wire and busbar (3, 4, 5 BB) schemes for finger width W_F = 65 μm. Multi-wire have been simulated assuming 82 fingers, while BB solar cells with an optimized number of fingers N_F.

This, in addition to the overall parasitic series resistance reduction, ensures an increase in efficiency in the case of encapsulated cells due to the advantages obtained in terms of optical interactions considering these materials (glass and encapsulant) in the electro-optical simulations.

Finally, Fig. 9a shows the paste consumption for four cases of finger width W_F with 3 BB, 4 BB, 5 BB (the optimum number of fingers N_F reported in this figure is calculated on the basis of the front grid parameters) and for the MW (the figure illustrates the optimum number of wires N_W and the wire diameter W_D).

It is worth noting that, overall the paste weight increases with increasing finger width. Hence, the decrease in the optimum number of fingers is associated to a widening of finger width which leads to an increase of paste volume. In addition, we observe that the relative gain in efficiency is higher for wider finger. The respective calculated efficiencies are shown in the Fig. 9b. Moreover, a decrease in maximum efficiency occurs for wider fingers due to Fill-Factor degradation.

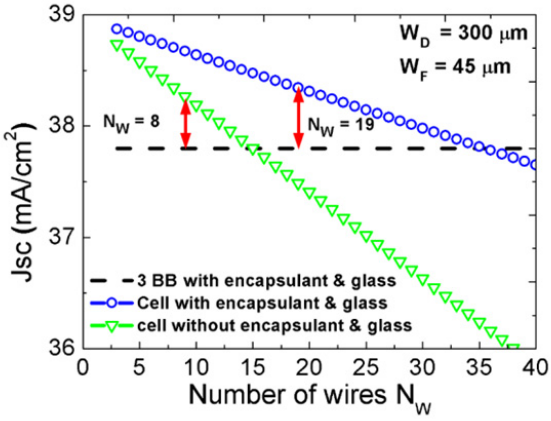

Fig. 8. Short circuit current J_{SC} versus number of wires for cell with encapsulant and glass or without encapsulant and glass. W_D denotes the wire diameter and W_F the finger width. A comparison with a three busbar (3 BB) solar cell is shown. The red arrows denote the gain in terms of J_{SC} (with respect to 3 BB) at the optimum number of wires N_W.

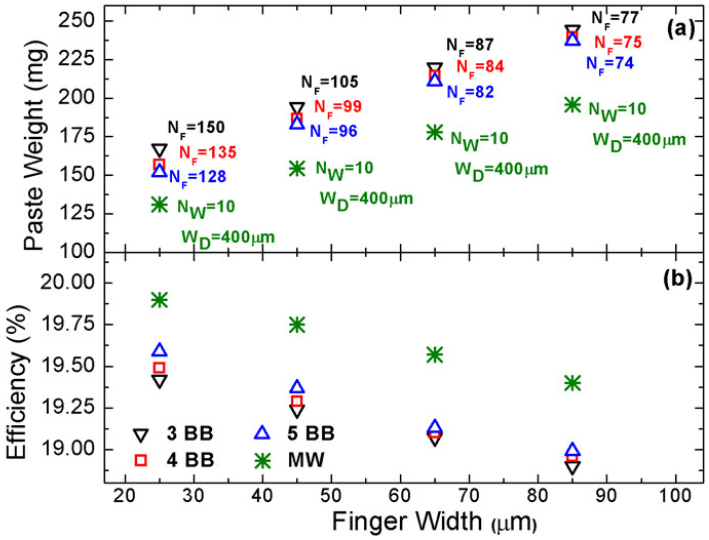

Fig. 9. Paste Weight (a) and efficiency (b) in the cases of multi-wire (MW) and busbar (3, 4, 5 BB) scheme for finger width W_F from 25 μm to 85 μm. N_F denotes the optimum number of fingers, N_W and W_D denote the optimum number of wires and the optimum wire diameter, respectively.

4. Conclusions

In this study, by using a ray-tracing simulation tool, we have analyzed the impact of geometries and optical properties of the materials on effective optical shading in the case of encapsulated industrial silicon solar cells which adopted multi-wire scheme. We have performed electro-optical simulations of MW and multi-busbar based solar cells in order to calculate the effective shading factor, the enhancement of efficiency and paste saving with respect to BB design. On the basis of our simulation study, such parameters have been revealed to be strongly dependent on the geometries of the encapsulant as well as on the optical reflectivity of the cell front interface. In particular, for encapsulant thickness close to the wire diameter, the effective optical shading is markedly dependent on the

encapsulant thickness. Instead, when the encapsulant thickness is much larger than the wire diameter we obtained an effective optical shading factor of 0.16 for planar front interface and of 0.22 for textured front interface. In addition, we observe that, at fixed CF, the effective optical shading is strongly dependent on the wire diameter. In particular, MW schemes take advantage of higher diameters, especially when CF is lower than 20 %. The calculated values of effective optical shading factor is 0.22 for CF up to 3 % independently of the wire diameter and 0.46 for lower wire diameter and CF = 10 % and these values are comparable to those reported in other works.

Indeed, although for a given CF higher W_D means a lower number of wires, the rounded cross section surface of the wire plays a role in lowering effective shading.

We have calculated the optimum number of wires at different diameters and compared the solar cell main figures of merit with those of the reference grid design assuming 3, 4, 5 silver BB. We observe that the most relevant resistance contribution is that of wire in the case of MW, while the finger resistance has minor impact. We note that the efficiency enhancement of the MW cell with respect to the BB option depends on wire diameter, fingers width and number of BB of the baseline.

In addition, we calculate an absolute enhancement of efficiency up to 0.5 $\%_{abs}$ with respect to the 3 BB design and a paste saving up to 50 mg in case of MW design, for the given cell design.

References

[1] Hannebauer H, Dullweber T, Falcon T, Chen X, Brendel R. Record low Ag paste consumption of 67.7 mg with dual print. Energy Procedia 2013;43:66-71.

[2] Zanuccoli M, Bresciani PF, Frei M, Guo HW, Fang H, Agrawal M, Fiegna C, Sangiorgi E. 2-D numerical simulation and modeling of monocrystalline selective emitter solar cells. 35th IEEE Photovoltaic Specialist Conference 2010;2262-2265.

[3] Braun S, Hahn G, Nissler R, Pönisch C, Habermann D. Multi-busbar solar cells and modules: high-efficiencies and low silver consumption. Energy Procedia 2013; 38:334-339.

[4] Braun S, Nissler R, Ebert C, Habermann D, Hahn G. High Efficiency Multi-busbar Solar Cells and Modules. IEEE Journal of Photovoltaics 2014; 4:148-153.

[5] Woehl R, Hörteis M, Glunz SW. Analysis of the Optical Properties of Screen-Printed and Aerosol-Printed and Plated Fingers of Silicon Solar Cells. Advances in OptoElectronics 2008; ID 759340.

[6] Blakers AW. Low loss metallisation of solar cells. Conference Record of the 23rd IEEE Photovoltaic Specialists Conference 1993;347-351.

[7] Paggi M, Corrado M, Rodriguez MA. A multi-physics and multi-scale numerical approach to microcracking and power loss in photovoltaic modules. Composite Structure 2013;95:630-638.

[8] Magnone P, De Rose R, Tonini D, Frei M, Zanuccoli M, Belli A, Galiazzo M, Sangiorgi E, Fiegna C. Numerical Simulation on the Influence of Via and Rear Emitters in MWT Solar Cells. IEEE Journal of Photovoltaics 2014;4:1032-1039.

[9] Sentaurus Device User Guide, Version C-2009.06. Synopsys. Inc., 2009.

[10] Enki Technology, 2192 Bering Drive, San Jose, CA 9513, 2014.

[11] McIntosh KR, Cotsell JN, Cumpston JS, Norris AW, Powell NE, Ketola BM. An optical comparison of silicone and EVA encapsulants for conventional silicon PV modules: A ray-tracing study. 34th IEEE Photovoltaic Specialist Conference, Philadelphia, 2009;544-549.

[12] ASTM Standard G173. Standard tables for reference solar spectral irradiances: direct normal and hemispherical on 37° tilted surface. Annual Book of ASTM Standards, vol. 12. 2008.

[13] Paternoster G, Zanuccoli M, Bellutti P, Ferrario L, Ficorella F, Fiegna C, Magnone P, Mettedi F, Sangiorgi E. Fabrication, characterization and modeling of a silicon solar cell optimized for concentrated photovoltaic applications. Solar Energy Materials and Solar Cells 2015;134:407-416.

[14] De Rose R, Zanuccoli M, Magnone P, Tonini D, Galiazzo M, Cellere G, Frei M, Guo HW, Fiegna C, Sangiorgi E. 2-D analysis of the impact of the highly-doped profile on selective emitter solar cell performance. 37th IEEE Photovoltaic Specialist Conference 2011;2556-2559.

[15] De Rose R, Van Wichelen K, Tous L, Das J, Dross F, Fiegna C, Lanuzza M, Sangiorgi E, Uruena De Castro A, Zanuccoli M. Optimization of rear contact geometry by means of 3-D numerical simulation. Energy Procedia 2012;27:197-202.

[16] Zanuccoli M, Michallon J, Semenihin I, Fiegna C, Kaminski-Cachopo A, Sangiorgi E, Vyrukov V. Numerical simulation of vertical silicon nanowires based heterojuntion solar cells. Energy Procedia 2013;38:216-222.

[17] Procel P, Maccaronio V, Crupi F, Cocorullo G, Zanuccoli M. Analysis of the impact of rear side geometry on performance of back-contact back-junction solar cells. Fotonica AEIT Italian Conference on Photonics Technologies, 2014; 6843919.

[18] De Rose R, Zanuccoli M, Magnone P, Sangiorgi E, Fiegna C. Open issue for the numerical simulation of silicon solar cells. 12th International Conference on Ultimate Integration on Silicon, ULIS 2011;1-4.

[19] Goetzberger A, Knobloch J, Voß B. Crystalline silicon solar cells. John Wiley & Sons, 1998.

[20] Green MA. Ag requirements for silicon wafer-based solar cells. Progress in Photovoltaics: Research and Applications 2011;8:911-916.

[21] Stuckings MF, Blakers AW. A study of shading and resistive loss from the fingers of encapsulated solar cells. Solar Energy Materials and Solar Cells 1999;59:233-242.